Modern Network Theory Design of Single-Sideband Crystal Ladder Filters

M. DISHAL, FELLOW, IEEE

Abstract—This paper presents modern network theory design data (rather than image parameter data) for one class of ladder network SSB crystal filters. The filter configuration involved uses crystals and capacitors only, so that the physical size of the resulting filters can be made quite small. A simple frequency transformation is first derived which enables the wealth of design data presently available for symmetrical response shape filters to be applied to the SSB response under consideration. It is shown that the transfer function being considered has n nonconjugate complex poles and n coincident zeros in the fractional bandwidth left half-plane. From the frequency transformation developed, graphs are presented for n-pole, n-coincident-zero SSB relative-attenuation shapes for $n=6$, 8, 10, and 12, with a pass band peak-to-valley ratio of zero decibels; and a computation example shows how graphs may be prepared for any n, and any pass band peak-to-valley ratio. Specific design equations are presented for all the elements involved in both the upper and lower SSB filter structures, and from these an equation is derived which shows how crystal units limit the maximum fractional bandwidth which can be obtained.

I. Introduction

WHEN, for reasons of system performance, it is desired to provide a high-rate-of-cutoff band-pass characteristic at such a mid-frequency that the ratio of this mid-frequency to the desired 3-dB bandwidth is of the order of 1000 or greater, then it is almost mandatory that crystal resonators be used in the filter. (This is true whether symmetrical or single-sideband (SSB) type of band-pass filtering is desired.)

When an SSB filter is required to pass the upper sideband, and the desired fractional pass band is as described previously, i.e. of the order of one part in one or two thousand, there is a particularly simple and practical crystals-and-capacitors-only ladder-type filter configuration which can be used to satisfy such a requirement; the ladder configuration is shown in Fig. 9. For lower sideband filters, the configuration is as shown in Fig. 10. As will be seen, for upper sideband filters, the ladder consists simply of crystal units plus shunting capacitors in the shunt arms, and capacitors only in the series arms; vice versa for lower sideband filters. These configurations were described as long ago as 1934 by Mason [1], and more recently in 1958 by Sykes [2]. To the best of the present author's knowledge, all the designs of these useful SSB filters have been based on image parameter theory, which means that the element values called for are based upon the use of physically unrealizable terminations, i.e., characteristic impedances.

Manuscript received October 19, 1964; revised March 18, 1965.
The author is with the ITT Federal Laboratories, Nutley, N. J.

It is the purpose of this paper to present for these ladder networks an "exact" modern network theory design, giving the element values required to obtain the exactly specified relative-attenuation shapes of which these SSB filters are capable.

Fig. 1(a) is a photograph of a lower sideband filter (on the left) and an upper sideband filter (on the right) of the type to be described, and illustrates the small physical size that results when crystals and capacitors only are required in a filter. Fig. 1(b) shows the swept relative attenuation of the upper sideband unit on a logarithmic-attenuation scale. The unit operates at 5 Mc/s; supplies a 3-dB-down bandwidth of 3.5 kc/s; has a sharp cutoff edge which falls to 60-dB relative attenuation in 560 c/s; provides 30-dB attenuation for the

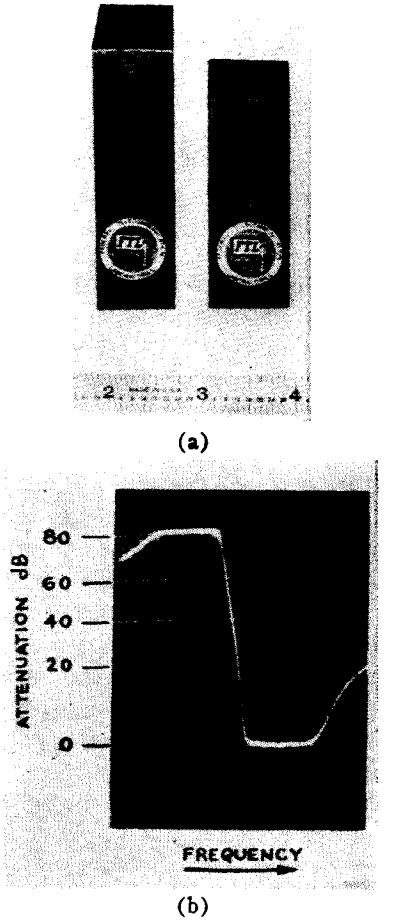

Fig. 1. (a) Lower (on left) and upper (on right) sideband crystals-and-capacitors-only SSB filters. (b) The swept relative attenuation on a logarithmic-attenuation scale of the upper sideband unit. The 80dB limitation is in the logarithmic measuring equipment, not in the filter.

carrier frequency; and maintains more than 60-dB rejection for two pass band widths below the carrier. The relative attenuation illustrated agrees with that foretold by the theory to be presented, with gratifying accuracy.

II. A Basic Ladder Network and its Generalized Relative-Attenuation Shape

Fig. 2 shows the basic node-type ladder, modification of which will produce the final crystals-and-capacitors-only upper sideband filter. In order to make sure that the reader realizes that no actual inductors will be required in the final network of Fig. 9, it is worth stressing here the fact that the inductors shown in Fig. 2 will, in a later design step, be absorbed in such a (proper) way that only crystals and capacitors remain in the final ladder.

In Fig. 2, each node is parallel-resonated to a frequency f_0 with all other nodes short-circuited; the lower case d's and k's are pure numerics commonly known as normalized decrements and normalized coefficients of coupling; G_1 and G_n are the conductances of the generator and load resistances; B_1 through B_n are the magnitudes of the equivalent capacitive (or inductive) susceptance of the respective ladder nodes at the node-resonant frequency; and B_{12} through $B_{(n-1)n}$ are the magnitudes of the susceptances of the respective coupling elements. In each coupling π the two inductors and one capacitor involved have the same susceptance magnitude, and it is assumed (realistically) that the percentage bandwidth of interest in the region of the mid-frequency is so small that the susceptance of any arm in the coupling mechanism changes negligibly with frequency.

If one solves for the complex transfer function of Fig. 2 by the straightforward application of Kirchhoff's Laws, the resulting equation takes the well-known form

$$\frac{\text{Output}}{\text{Input}} = \frac{c}{(jv)^n + u_{(n-1)}(jv)^{n-1} + u_{(n-2)}(jv)^{(n-2)} + \cdots u_0} \quad (1)$$

where the coefficients (u's) are pure real numbers made up of various combinations of the d's and k's, and having values such that $n/2$ conjugate complex pairs of poles can be obtained for n even; and $(n-1)/2$ conjugate pairs and one real pole can be obtained for n odd.

Over the last 25 years, a large body of knowledge has evolved concerning the relative-attenuation shapes which can be obtained from networks supplying such transfer function poles; and it is now well known that vs. the generalized frequency variable v, Butterworth, Chebyshev, maximally linear phase, Gaussian magnitude, etc., are some of the useful relative-attenuation shapes that can be obtained by proper location of the transfer function poles in the jv plane [3]–[5].

The relative-attenuation shape given at the bottom of Fig. 2 is the Chebyshev shape; but the reader will realize that the other shapes mentioned in the preceding paragraph can also be obtained as a function of the general variable v.

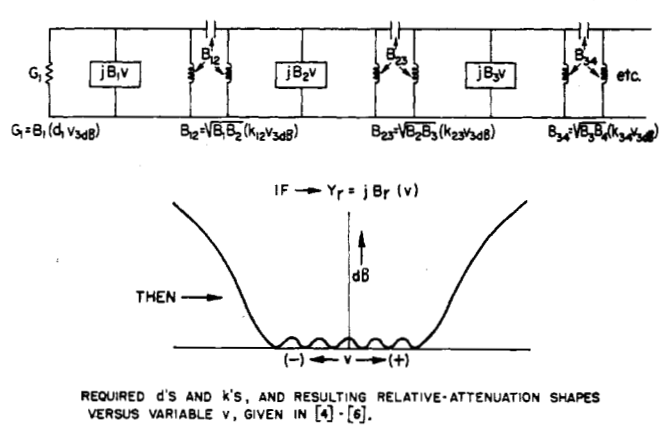

Fig. 2. The basic small-percentage-bandwidth node network and its resulting symmetrical relative-attenuation shape. (It is important to realize that the inductors shown are properly absorbed in a later design step, so that in the final network of Fig. 9 no physical inductors are required.)

For the network designer, the proper locations of the complex frequency poles are only a means to an end; the end being the proper element values in his network. As will be seen from Fig. 2, the normalized decrements (d's) and normalized coefficients of coupling are one set of constants which give the network designer immediately applicable design information for obtaining his required element values. By means of the well-known Darlington procedure [3], [6], or any equivalent procedure, one can obtain the required network d's and k's for any and all of the previously mentioned relative-attenuation shapes, and because the information is obtained in normalized form, the large amount of work involved need only be done once by some person or group, and then should properly be considered a piece of available knowledge. These required $d(=1/q)$ and k values have been given [4], [6] for the symmetrical Butterworth, Chebyshev, and maximally linear phase responses [4], [6], and for the symmetrical Gaussian magnitude response [5]. In addition, the detailed characteristics of the various symmetrical relative-attenuation shapes have been given in these references. It should be realized, however, that in these references, the abscissas of the relative-attenuation graphs are labelled in terms of actual frequency, whereas for the purpose of this paper these abscissas must be considered to be a generalized variable v.

Because of space restrictions, this large amount of available information will not be repeated in this paper, and it will be assumed that the reader will make use of the appropriate reference. However, to complement the relative-attenuation examples to be presented as Figs. 5–8 of this paper, Tables I and II are introduced, giving (from these references) the d's and k's required to produce a pass band which is maximally flat (Table I), and one having a peak-to-valley ratio of 0.1 dB (Table II).

TABLE I

3-dB Bandwidth Normalized d's and k's Required to Produce a Maximally-Flat Pass Band

n	6	8	10	12
d_1	1.93	2.56	3.20	3.83
k_{12}	1.17	1.52	1.88	2.24
k_{23}	0.606	0.734	0.883	1.036
k_{34}	0.518	0.551	0.630	0.719
k_{45}	0.606	0.510	0.533	0.585
k_{56}	1.17	0.551	0.507	0.522
k_{67}		0.734	0.533	0.504
k_{78}		1.53	0.630	0.522
k_{89}			0.883	0.585
$k_{9,10}$			1.88	0.719
$k_{10,11}$				1.036
$k_{11,12}$				2.24
d_n	1.93	2.56	3.20	3.83

TABLE II

3-dB Bandwidth Normalized d's and k's Required to Produce a Pass Band Peak-to-Valley Ratio of 0.1 dB

n	6	8	10	12
d_1	0.788	0.796	0.805	0.811
k_{12}	0.716	0.727	0.734	0.739
k_{23}	0.539	0.545	0.550	0.551
k_{34}	0.518	0.516	0.519	0.521
k_{45}	0.539	0.510	0.509	0.510
k_{56}	0.716	0.516	0.506	0.506
k_{67}		0.545	0.509	0.504
k_{78}		0.727	0.519	0.506
k_{89}			0.550	0.510
$k_{9,10}$			0.734	0.521
$k_{10,11}$				0.551
$k_{11,12}$				0.739
d_n	0.788	0.796	0.805	0.811

III. The Frequency Variable for a Crystal Shunt Arm

As pointed out in Section II and Fig. 2, a large body of already known detailed design data can be made use of for designing band-pass networks in the form of Fig. 2, if the admittance of all the shunt arms being used can be written in the form

$$Y = jB_r v \tag{2}$$

with all the terms involving variable actual frequency being contained in the factor v.

As an example, let us take the well-known symmetrical band-pass case obtained when the shunt arms consist of simple parallel-resonant circuits, as shown in the top part of Fig. 3. The admittance of this simple arm is given by

$$Y = j\omega_0 C\left(\frac{\omega}{\omega_0} - \frac{\omega_0}{\omega}\right) \tag{3}$$

and for the small-percentage-bandwidth case being considered in this paper, wherein $0.95 < (\omega/\omega_0) < 1.05$, it is well known that the bracketed geometrically symmetrical frequency variable of (3) approaches the linear fractional bandwidth variable of (4),

$$\left(\frac{\omega}{\omega_0} - \frac{\omega_0}{\omega}\right) \doteq 2\frac{(f - f_0)}{f_0} \equiv F. \tag{4}$$

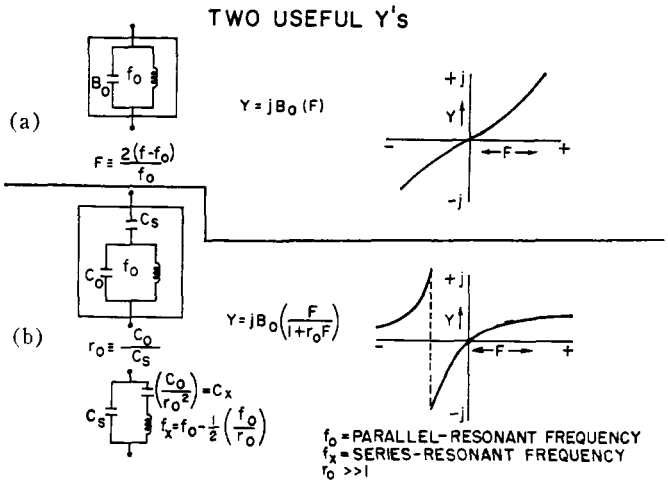

Fig. 3. (a) A simple admittance often used for the network of Fig. 2. (b) An admittance similar in form to that of a crystal unit.

Thus, if simple parallel-resonant arms are used in the network of Fig. 2, a comparison of (2) and (3) shows that the relationship between the symmetrical general variable v and actual frequency is given by

$$v = \frac{2(f - f_0)}{f_0} \equiv F. \tag{5}$$

Now, let us obtain the relationship between our general symmetrical variable v and actual frequency when a crystal unit is used for the shunt arms of the network of Fig. 2. The bottom part of Fig. 3 shows the two equivalent circuits for such an element and, with the realistic approximation that $r_0 \gg 1$, gives the relationships between the various element values in the two equivalences. Straightforward Kirchhoff Law analysis for the admittance of such an arm results in

$$Y = j\omega_0 C_0 \left\{ \frac{\left(\frac{\omega}{\omega_0} - \frac{\omega_0}{\omega}\right)}{1 + \left(\frac{C_0}{C_s}\right)\left(\frac{\omega_0}{\omega}\right)\left(\frac{\omega}{\omega_0} - \frac{\omega_0}{\omega}\right)} \right\} \tag{6}$$

and for the small-percentage-bandwidth case being considered in this paper, wherein $0.95 < (\omega/\omega_0) < 1.05$, (6) may be written as

$$Y = j\omega_0 C_0 \left(\frac{F}{1 + r_0 F}\right) \tag{6a}$$

where F is the frequency function given in (4), r_0 is the ratio of C_0 to C_s in the first equivalent circuit, and C_0 is as shown in the first equivalent circuit.

For small-percentage-bandwidth networks, the actual frequency variable which is most useful to the designer is the much-used fractional bandwidth variable of (4), and, through the medium of (6), Fig. 3 shows the way the admittance of the crystal arm varies vs. this frequency variable F.

Comparison of (2) and (6) gives us (7), the relation-

ship between our general variable v and actual fractional bandwidth,

$$v = \frac{F}{1 + r_0 F}. \tag{7}$$

A. Transfer Function Poles and Zeros on the Fractional Bandwidth Plane

If (7) is substituted in (1), we will then obtain the transfer function produced by this network in terms of the desired fractional bandwidth variable. The resulting equation has a denominator which is a polynomial in terms of (jF), of highest power n, where n is the number of crystals used, and with complex coefficients rather than pure real coefficients; the resulting numerator of this transfer function is not a constant, but is $(1+r_0F)^n$.

The numerator just described means that there are n-coincident real frequency transfer function zeros supplied by this network; and the denominator just described means that there are n complex left half-plane transfer function poles supplied by this network. The fact that the coefficients of the denominator polynomial are complex, means that these n poles do *not* occur in conjugate complex pairs; each pole has both a real and an imaginary coordinate which is different from those for any other pole. However, there are still n of these poles laid down in the left half of the $[jF/(BW_3/f_0)]$ plane, and therefore it is proper to classify the nonsymmetrical SSB response involved as an n-poles, n-coincident-zeros transfer function, where n is the number of crystals used.

By substituting the well-known pole locations for the symmetrical Butterworth and Chebyshev [7], linear phase [8], Gaussian [5], etc. response shapes in (9) (to be developed in the next section), the reader can obtain numerical values for the left half-plane SSB pole locations on the $jF/(BW_3/f_0)$ plane. These transformed pole locations will produce the SSB relative-attenuation shapes to be described in the following section. Versus actual bandwidth, the transformed linear phase and Gaussian shapes will, of course, no longer be linear phase or Gaussian. Reference to these shapes is included because the resultant transformed shapes may prove to be useful.

IV. The Resulting Upper Sideband Filter Relative-Attenuation Shape

A. Equations Related to f_0

To obtain the relationship between fractional bandwidth and the symmetrical variable v, we merely solve (7) for F and obtain

$$F = \frac{v}{1 - r_0 v}. \tag{7a}$$

Relative-attenuation plots must, of course, be normalized to some clearly defined reference bandwidth; one of the most common and useful of these is the 3-dB-down bandwidth, which we will use.

At the 3-dB-down point, the general symmetrical variable v is given the subscript v_3, and the corresponding fractional bandwidth will be

$$F_3 = \frac{v_3}{1 - r_0 v_3} \tag{7b}$$

where both v_3 and F_3 are algebraic.

To obtain the equation for the total 3-dB-down bandwidth, we add the two magnitudes obtained from (7b); when v_3 is first made positive to obtain the upper 3-dB fractional bandwidth, and is then made negative to obtain the lower 3-dB-down fractional bandwidth.

The resulting expression is given by

$$\frac{BW_3}{f_0} = \frac{|v_3|}{1 - |r_0 v_3|^2}. \tag{8}$$

Dividing (7a) by (8) we obtain the normalized transformation equation

$$\frac{F}{BW_3/f_0} \equiv \frac{f - f_0}{BW_3/2} \equiv \frac{\Delta f_0}{BW_3/2} = \frac{1 - |r_0 v_3|^2}{\frac{|v_3|}{v} - |r_0 v_3|}. \tag{9}$$

Equation (9) enables us to take all the symmetrical relative-attenuation plots given in the literature for Butterworth, Chebyshev, maximally linear phase, Gaussian amplitude, etc. and transform them into the upper sideband relative attenuations which result when crystal units are used in the network of Fig. 2. As previously noted, when this is done the resulting pass bands are no longer linear phase or Gaussian vs. actual bandwidth.

Remembering that the general band-pass frequency variable v is algebraic, and that it is positive above the resonant frequency and negative below resonance, examination of (9) shows that the SSB relative attenuation is laid down in three distinct regions.

These three regions are detailed in Fig. 4, which shows graphically the relationship between the already published symmetrical relative-attenuation graphs and the upper sideband relative-attenuation curves into which they can be transformed.

Notice that in (9) and in Fig. 4 the quantity $1/r_0v_3$ has been maintained as one entity. We see from Fig. 4 that this quantity sets the location of the frequency of infinite rejection and, as we will see later, it is an important parameter whose value the filter designer must pick.

B. Equations Related to the Arithmetic Middle of the 3-dB-Down Bandwidth

When dealing with a single-sideband filter specification, the node-resonant frequency (f_0) is, in general, never specified; instead the two frequencies defining the edges of the pass band are specified. As already noted, in this paper we are using the 3-dB-down bandwidth as the normalizing bandwidth, and it would be most conven-

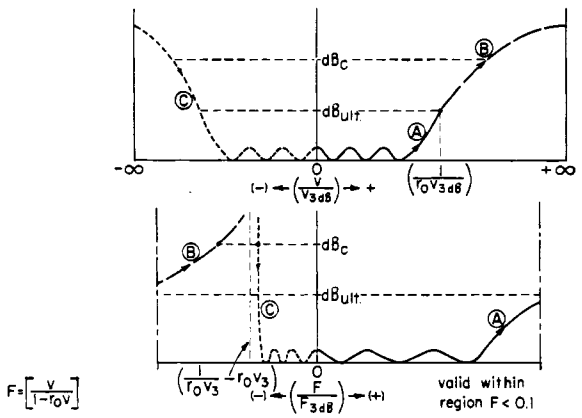

Fig. 4. The manner in which (9) transforms the symmetrical relative-attenuation shapes of [4]–[6] into an upper SSB relative-attenuation shape.

ient, therefore, to express the various frequency relationships in terms of frequency deviations from the arithmetic middle of this 3-dB-down pass band. The simple relationship between the two 3-dB-down frequencies, the half-bandwidth ($BW_3/2$), and the arithmetic mid-frequency is given by

$$f_m = f_{3_L} + \left(\frac{BW_3}{2}\right) = f_{3_H} - \left(\frac{BW_3}{2}\right). \tag{10}$$

To obtain (9), in terms of the arithmetic mean frequency f_m, we must first obtain an expression for f_{3_L} or f_{3_H} in terms of f_0 and $BW_3/2$. Equation (9) with v/v_3 set equal to -1.0 and $+1.0$, respectively, gives the required expressions, which are

$$f_0 = f_{3_H} - \left(\frac{BW_3}{2}\right)[1 + |r_0 v_3|] \tag{11}$$

and

$$f_0 = f_{3_L} + \left(\frac{BW_3}{2}\right)[1 - |r_0 v_3|]. \tag{12}$$

Finally, either (11) or (12) in conjunction with (8) results in (13), which gives the relationship between the resonant frequency (f_0) and the arithmetic mean frequency f_m,

$$f_m = f_0 + \left(\frac{BW_3}{2}\right)|r_0 v_3|. \tag{13}$$

We can now substitute (13) into (9) to obtain (14), the normalized transformation equation in terms of the arithmetic mean frequency f_m,

$$\frac{f - f_m}{BW_3/2} \equiv \frac{\Delta f_m}{BW_3/2} = \frac{\left|\frac{1}{r_0 v_3}\right|\frac{v}{|v_3|} - 1}{\left|\frac{1}{r_0 v_3}\right| - \frac{v}{|v_3|}}. \tag{14}$$

For the three regions shown in Fig. 4, the magnitude of (14) can be written as:

For Region A (the slow cutoff side),

$$0 < \left(\frac{v}{v_3}\right) < + \left|\frac{1}{r_0 v_3}\right|$$

and

$$-|r_0 v_3| < \left(\frac{\Delta f_m}{BW_3/2}\right) < (+\infty)$$

and the magnitude of (14) can be written as

$$\left|\frac{f - f_m}{BW_3/2}\right|_A = \frac{\left|\frac{1}{r_0 v_3}\right|\left|\frac{v}{v_3}\right| - 1}{\left|\frac{1}{r_0 v_3}\right| - \left|\frac{v}{v_3}\right|}. \tag{14a}$$

For Region B (the "return hill" portion of the relative attenuation),

$$+\left|\frac{1}{r_0 v_3}\right| < \left|\frac{v}{v_3}\right| < + \infty$$

and

$$(-\infty) < \left(\frac{\Delta f_m}{BW_3/2}\right) < -\left|\frac{1}{r_0 v_3}\right|$$

and the magnitude of (14) can be written as

$$\left|\frac{f - f_m}{BW_3/2}\right|_B = \frac{\left|\frac{1}{r_0 v_3}\right|\left|\frac{v}{v_3}\right| - 1}{\left|\frac{v}{v_3}\right| - \left|\frac{1}{r_0 v_3}\right|}. \tag{14b}$$

Finally, for Region C (the sharp cutoff edge),

$$-\infty < \left(\frac{v}{v_3}\right) < 0$$

and

$$-\left|\frac{1}{r_0 v_3}\right| < \left(\frac{\Delta f_m}{BW_3/2}\right) < -|r_0 v_3|,$$

and the magnitude of (14) can be written as

$$\left|\frac{f - f_m}{BW_3/2}\right|_C = \frac{\left|\frac{1}{r_0 v_3}\right|\left|\frac{v}{v_3}\right| + 1}{\left|\frac{1}{r_0 v_3}\right| + \left|\frac{v}{v_3}\right|}. \tag{14c}$$

Transformation equations (14a)–(14c), in conjunction with the symmetrical variable relative-attenuation curves and equations of [4] and [5], have been used to plot the SSB relative-attenuation graphs of Figs. 5–8.

Table III is an example of the computations involved in preparing these curves; and, through construction of similar tables, the reader can prepare relative-attenuation graphs for this n-pole, n-coincident-zeros family of SSB attenuations for any chosen n, pass band ripple, and $1/r_0 v_3$.

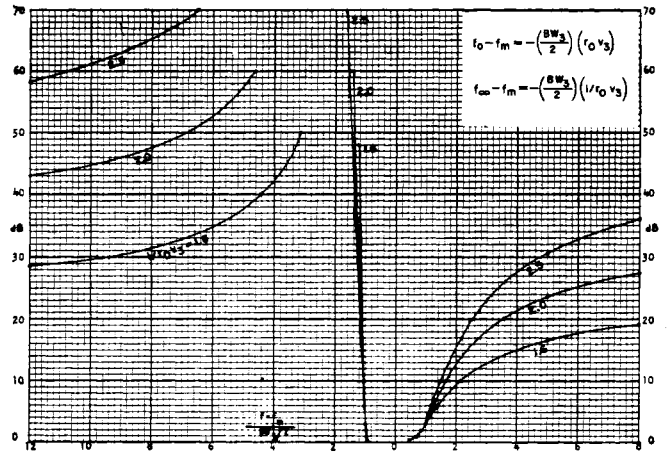

(a)

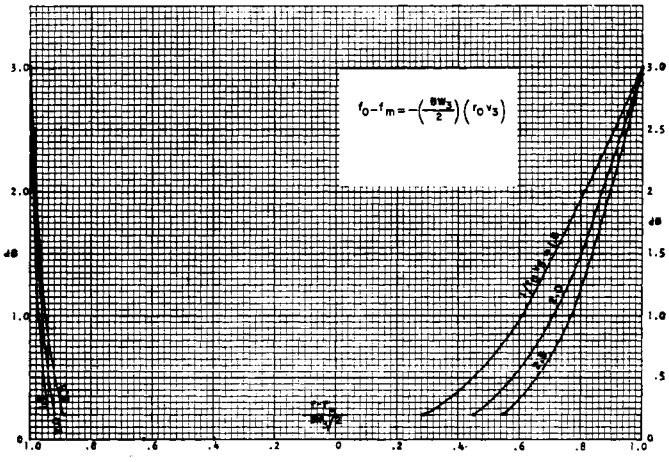

(b)

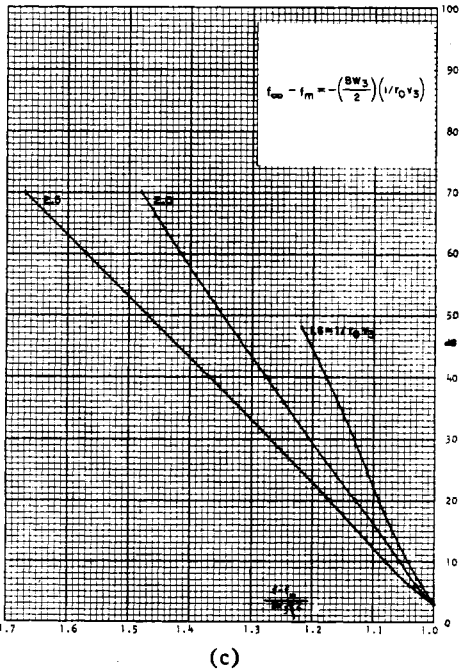

(c)

Fig. 5. (a) 6-pole, 6-coincident-zero SSB relative-attenuation shape ($V_p/V_v = 0$ dB). (b) Expanded relative attenuation inside the 3-dB-down points. (c) Expanded relative attenuation of sharp cutoff edge.

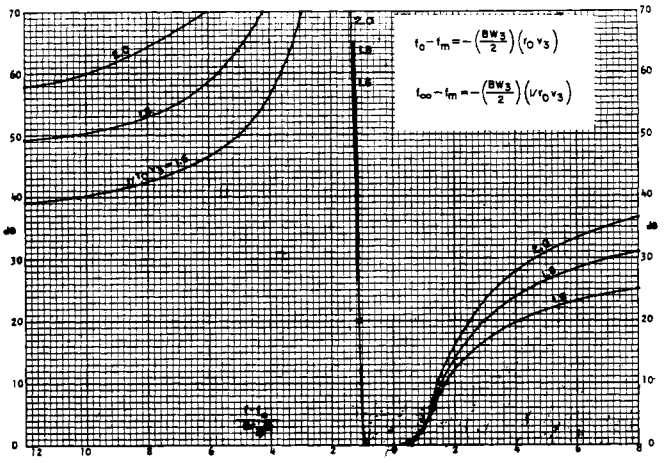

(a)

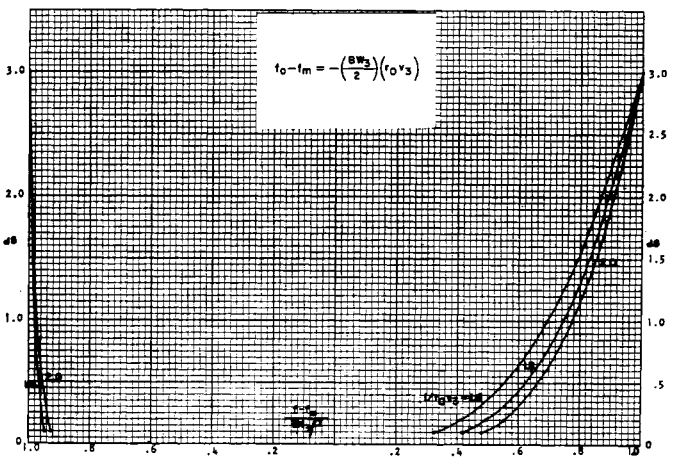

(b)

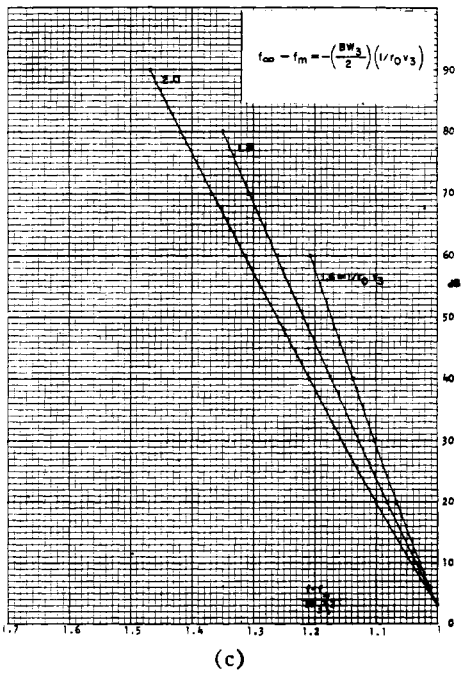

(c)

Fig. 6. (a) 8-pole, 8-coincident-zero SSB relative attenuation shape ($V_p/V_v = 0$ dB). (b) Expanded relative attenuation inside the 3-dB-down points. (c) Expanded relative attenuation of sharp cutoff edge.

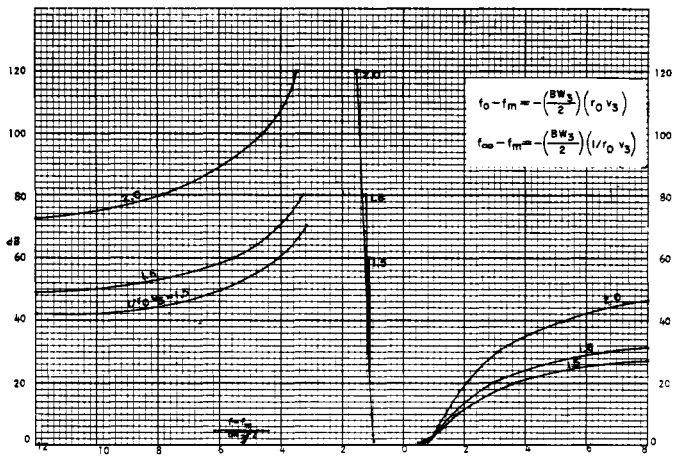

(a)

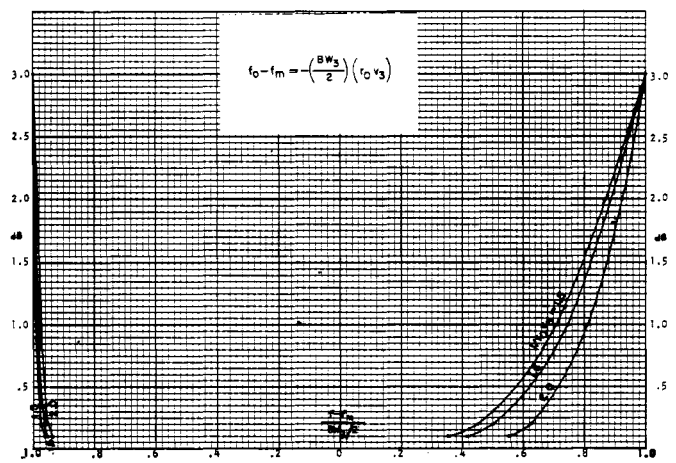

(b)

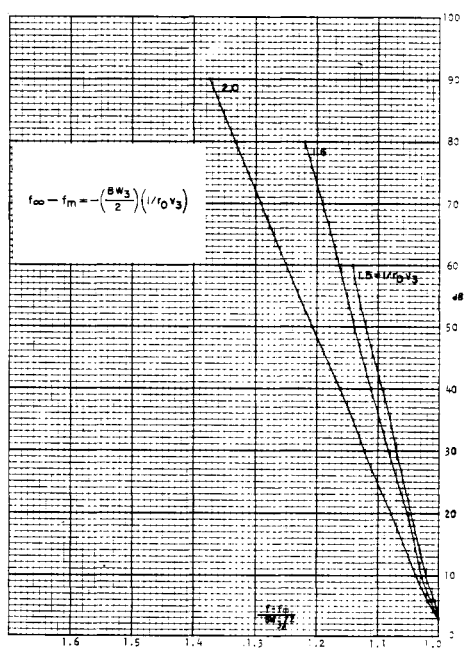

(c)

Fig. 7. (a) 10-pole, 10-coincident-zero SSB relative attenuation shape ($V_p/V_r = 0$ dB). (b) Expanded relative attenuation inside the 3-dB-down points. (c) Expanded relative attenuation of sharp cutoff edge.

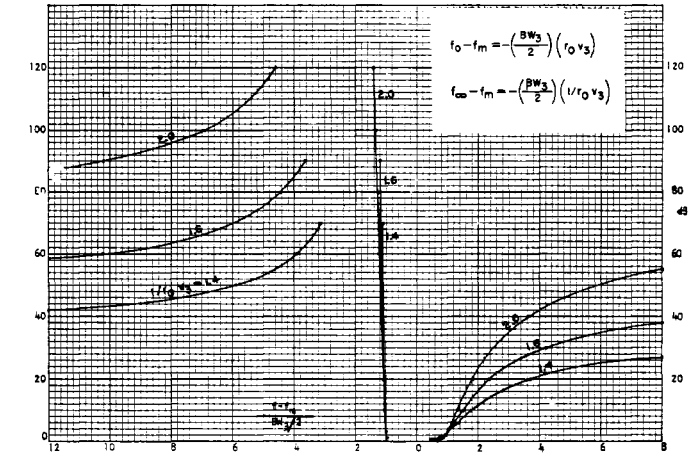

(a)

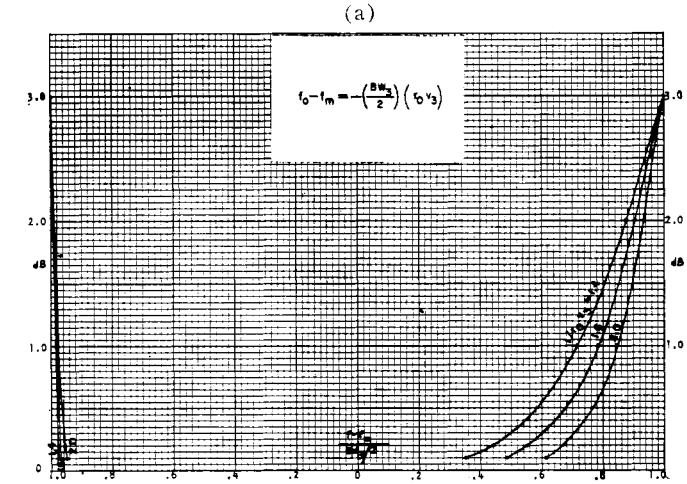

(b)

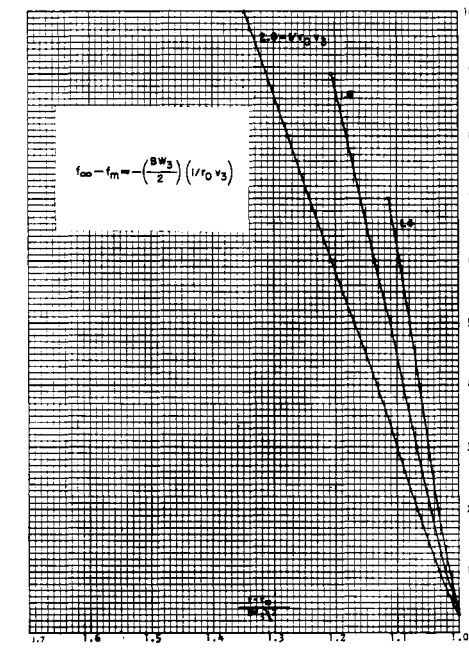

(c)

Fig. 8. (a) 12-pole, 12-coincident-zero SSB relative-attenuation shape ($V_p/V_r = 0$ dB). (b) Expanded relative attenuation inside the 3-dB-down points. (c) Expanded relative attenuation of sharp cutoff edge.

TABLE III

COMPUTATION EXAMPLE FOR 10-POLES, 10-COINCIDENT-ZEROS SSB RELATIVE ATTENUATION FOR $V_p/V_v=0$ dB AND $1/r_0v_3=1.6$

From [4] dB	From [4] $\left(\frac{v}{v_3}\right)\equiv X$	Slow cutoff side $\frac{1.6X-1}{1.6-X}$	Return hill $\frac{1.6X-1}{X-1.6}$	Sharp cutoff edge $\frac{1.6X+1}{1.6+X}$
0	0	−0.625		0.625
0+	0.625	0		0.888
.1	0.826	0.415		0.957
.2	0.859	0.502		0.965
1	0.935	0.746		0.985
2	0.973	0.887		0.992
3	1.000	1.000		1.000
6	1.056	1.270		1.012
10	1.116	1.628		1.029
20	1.258	2.953		1.052
30	1.411	6.66		1.082
40	1.586	109.6		1.110
	1.60	∞	∞	1.111
50	1.779		10.30	1.140
60	1.994		5.56	1.165
70	2.24		4.40	1.191
80	2.515		3.32	1.220
∞	∞		1.60	1.60

It may be helpful at this point to obtain the exact relationship between the important parameter $1/r_0v_3$ and the location of the infinite-attenuation point. From Fig. 4 we see that infinite attenuation is reached when the symmetrical variable $|v/v_3|$ equals infinity; inserting this value for v/v_3 in (14) results in

$$\frac{f_m-f_\infty}{BW_3/2}=\left|\frac{1}{r_0v_3}\right|. \tag{15}$$

Thus, we see that the parameter $1/r_0v_3$ sets directly the ratio of the bandwidth between the infinite-attenuation frequency and the center of the pass band to the 3-dB-down half-bandwidth.

Since with this particular SSB filter all the crystals are series resonant at the frequency of infinite attenuation, the solution of (15) will produce (15a), the design equation which will specify the required crystal series-resonant frequency,

$$f_\infty=f_m-\left(\frac{BW_3}{2}\right)\left|\frac{1}{r_0v_3}\right|. \tag{15a}$$

For a given number of crystals (n) and a given peak-to-valley ratio (V_p/V_v), there is another characteristic of the relative attenuation which is immediately set when the parameter $1/r_0v_3$ is chosen; this is the ultimate attenuation (Db_u), which will be approached far from the pass band, but still within the small-percentage-bandwidth region. As Fig. 4 shows, this ultimate attenuation occurs at the transition point between Region A and Region B, i.e., when (16) applies,

$$\left|\frac{v}{v_3}\right|_{Db_u}=\left|\frac{1}{r_0v_3}\right|. \tag{16}$$

Thus on the symmetrical relative-attenuation graphs, or equations, of [4] and [5], the decibel attenuation obtained when the abscissa has the value $1/r_0v_3$ is the ultimate attenuation that the chosen n, (V_p/V_v), and $1/r_0v_3$ can approach in the small-percentage-bandwidth region.

C. A Method for Obtaining the Required $1/r_0v_3$

The graphs of Figs. 5–8 enable an engineer to start his design by picking the approximate number of crystals required to satisfy his particular SSB filter specification. To arrive at the exact value of $1/r_0v_3$ and (V_p/V_v), and at the exact number of crystals required, the following procedure may be used

Step 1. Given:

a) Required decibel attenuation (dB_c) at a specified bandwidth $(f_m-f_c)\equiv\Delta f_c$ on the sharp cutoff edge.

b) Required ratio of Δf_c to $BW_3/2$.

Pick:

c) Number of crystals.

d) Pass band ripple.

Step 2. From the relative-attenuation curves, or equations, of [4] or [5] obtain the corresponding $|v/v_3|_c$.

Step 3. Calculate required $1/r_0v_3$ from (17).

$$\left|\frac{1}{r_0v_3}\right|=\frac{\left(\frac{\Delta f_c}{BW_3/2}\right)\left|\frac{v}{v_3}\right|-1}{\left|\frac{v}{v_3}\right|_c-\frac{\Delta f_c}{BW_3/2}} \tag{17}$$

Because it is the sharp cutoff edge that is involved in these steps, (17) is obtained simply by solving (14c) for $1/r_0v_3$.

Step 4. Use (14b) to determine at what bandwidth on the return hill the specified decibel rejection is obtained, when the $1/r_0v_3$ of Step 3 is used.

$$\frac{\Delta f_B}{BW_3/2}=\frac{\left|\frac{1}{r_0v_3}\right|\left|\frac{v}{v_3}\right|_c-1}{\left|\frac{v}{v_3}\right|_c-\left|\frac{1}{r_0v_3}\right|} \tag{14b}$$

If this reject bandwidth is too narrow, then a larger peak-to-valley ratio in the pass band or a larger number of crystals must be picked, and Steps 1 through 4 repeated, until the required reject bandwidth is obtained.

V. REQUIRED UPPER-SIDEBAND NETWORK ELEMENT VALUES WHEN ALL CRYSTALS ARE IDENTICAL

It has already been pointed out that for the simple SSB shape being considered, all the crystals being used have the same series-resonant frequency given by (13a). For ease of manufacture, it would be highly desirable that all the crystals used also have the same motional capacitance C_x.

From the equivalence shown in Fig. 3, we see that the

admittance of the motional capacitance of the crystal unit is related to the node admittance level B_0 by

$$B_x = \frac{B_0}{r_0^2}. \tag{18}$$

Thus, for all the crystals to have the same required motional capacitance, we see that B_1, B_2, B_3, etc. in Fig. 2 must have the same value for each node (since, as has already been pointed out, r_0 sets the location of the infinite-attenuation frequency, which frequency is identical for each node).

We can now return to Figs. 2 and 3 and substitute in the general element value equations given there. We see from Figs. 2 and 3 that equations will be required for v_3 and r_0; let us now obtain these. v_3 is obtained directly by solution of (8) to obtain

$$|v_3| = \left(\frac{BW_3}{f_0}\right)[1 - |r_0 v_3|^2]. \tag{19}$$

Dividing the product $r_0 v_3$ by (19) will, of course, give r_0; we thus obtain

$$r_0 = \left(\frac{f_0}{BW_3}\right) \Big/ \left[\left|\frac{1}{r_0 v_3}\right| - |r_0 v_3|\right]. \tag{20}$$

A. The Required Loading Resistors

Returning to Fig. 2 we see that the required conductance of the first node loading resistor is given by

$$G_1 = d_1 B_1 |v_3| \tag{21}$$

where $d_1 (= 1/q_1)$ is given in the design tables [4]–[6], B_1 is the B_0 of (18), and v_3 and r_0 are given by (19) and (20), respectively. Substitution of these equations in (21) results in our first network design equation,

$$\frac{G_1}{B_x} = d_1 \frac{(f_0/BW_3)}{\left[\left|\frac{1}{r_0 v_3}\right|^2 - 1\right]}. \tag{22}$$

The design equation for the conductance G_n of the required loading resistor across node n will be identical in form, with G_n replacing G_1, and d_n replacing d_1.

B. The Required Coupling Capacitors

Again returning to Fig. 2, we see that the required susceptance of the first coupling capacitor is given by

$$B_{12} = k_{12}\sqrt{B_1 B_2}\,|v_3| \tag{23}$$

where k_{12} is given in the design tables and equations of [4]–[6].

Substituting (18)–(20) into (23) produces the second design equation,

$$\frac{C_{12}}{C_x} = k_{12} \frac{(f_0 | BW_3)}{\left|\frac{1}{r_0 v_3}\right|^2 - 1}. \tag{24}$$

An equation of identical form will be obtained from the required value of the other coupling capacitors, with C_{23}, C_{34}, etc. replacing C_{12}, and k_{23}, k_{34}, etc. replacing k_{12}.

C. The Required Crystal Series-Resonant Frequency

It has already been pointed out that in this network the frequency of infinite attenuation is the series-resonant frequency of each crystal. This frequency of infinite attenuation is given by (15a) and, therefore, the design equation for series-resonant frequency of every crystal is

$$f_x = f_m - \left(\frac{BW_3}{2}\right)\left(\frac{1}{r_0 v_3}\right). \tag{25}$$

To give the required crystal series-resonant frequency in terms of the specified 3-dB-down point on the sharp cutoff edge, (10) is substituted into (25) to obtain

$$f_x = f_{3dB_L} - \left(\frac{BW_3}{2}\right)\left[\left|\frac{1}{r_0 v_3}\right| - 1\right]. \tag{26}$$

D. The Required Shunt Capacitances Across Each Node

Inside each shunt-arm box in the network of Fig. 2 there would be placed the bottom equivalent circuit of Fig. 3. We see, therefore, that inside each box there would appear a capacitance (C_s) shunting the series-resonant circuit, and from the definition of r_0 given in Fig. 3, the value of C_s would be obtained from

$$C_s = \frac{C_0}{r_0} = r_0 C_x. \tag{27}$$

It is important to realize that C_s is not the shunt capacitance to be used in the real-life network. As can be seen from Fig. 2, this capacitance C_s, inside each box, is shunted by two inductors, one from the coupling π preceding it, and one from the coupling π following it. Over the small-percentage bandwidth involved in these filters, the resultant susceptance of this parallel combination can be approximated by a new capacitance of susceptance.

$$B_{p_1} = r_0 B_x - B_{12} \tag{28a}$$

$$B_{p_2} = r_0 B_x - (B_{12} + B_{23}) \tag{28b}$$

$$B_{p_3} = r_0 B_x - (B_{23} + B_{34}) \tag{28c}$$

etc.

If we now substitute (20) and (24) in the preceding equations, we obtain our desired design equation,

$$\frac{C_{p_2}}{C_x} = \left(\frac{f_0}{BW_3}\right)\left\{\frac{\left|\frac{1}{r_0 v_3}\right| - (k_{12} + k_{23})}{\left|\frac{1}{r_0 v_3}\right|^2 - 1}\right\} \tag{29}$$

and an identical equation in form will be obtained for the required value of each shunt capacitance, with C_{p_1} replacing C_{p_2}, and $(0 + k_{12})$ replacing $(k_{12} + k_{23})$, etc.

C_{p_r} is the required shunt capacitance value which must be placed across the rth-series resonance, and, of course, to find the value of the actual physical capacitor which must be added across each crystal unit, the crystal holder capacitance (C_h) would be subtracted from each C_p.

The resulting crystals-and-capacitors-only network, and the preceding design equations are shown in Fig. 9.

Another method for obtaining the required value of each C_p is contained in the statement at the bottom of Fig. 9. The statement is based upon the following fact: If we calculate C_t, the sum of the three capacitors which touch each node, i.e., $(C_{12}+C_{p_2}+C_{23})$ for node 2 for example, we obtain the fact that for every node

$$\frac{C_t}{C_x} = r_0 = \frac{(f_0/BW_3)}{\left|\frac{1}{r_0 v_3}\right| - |r_0 v_3|} \tag{30}$$

i.e., the total capacitance touching each node (excluding the series-resonant circuit) is a constant of value given by (30). This fact can also be used as a convenient double check of the numerical design work.

It is worth presenting another viewpoint concerning the function of the shunt capacities C_{p_1}, C_{p_2}, etc. in the network of Fig. 9. In the straightforward node network involved, the parallel-resonant frequency (f_0) of each node, with every other node short-circuited, must be the same; and in terms of the specified edges of the pass band, (11) and (12) give the required value of this node parallel-resonant frequency (f_0), with all other nodes short-circuited. The values of C_{p_1}, C_{p_2}, etc., as given by (29) or (30), produce this correct node parallel resonance.

E. Maximum Physically Realizable Bandwidth

By their nature, crystal units inherently possess a certain minimum possible ratio of holder to motional capacitance (C_h/C_x); for example, a minimum possible value of approximately 200 is practical for AT cut crystals in the 5-Mc/s region. In the network of Fig. 9, it is obvious that the lowest value that can be demanded of any C_p is the capacitance C_h of the crystal unit being used. Equation (29) is thus a powerful one for determining the maximum fractional bandwidth which can be obtained with a desired shape and specified crystal units. Solving (29) for (BW_3/f_0) and substituting $(C_h/C_x$ for C_p/C_x, we obtain

$$\left(\frac{BW_3}{f_0}\right)_{\text{max. possible}} = \left(\frac{C_x}{C_h}\right)\left\{\frac{\left|\frac{1}{r_0 v_3}\right| - (k_{12}+k_{23})}{\left|\frac{1}{r_0 v_3}\right|^2 - 1}\right\}. \tag{31}$$

A numerical example of the usefulness of this equation is worthwhile. Let us consider the case wherein a specified SSB requirement can be satisfied by the relative attenuation produced by that 6-pole, 6-zero maximally-flat pass band curve of Fig. 5, having $1/r_0 v_3$ equal to 2.5.

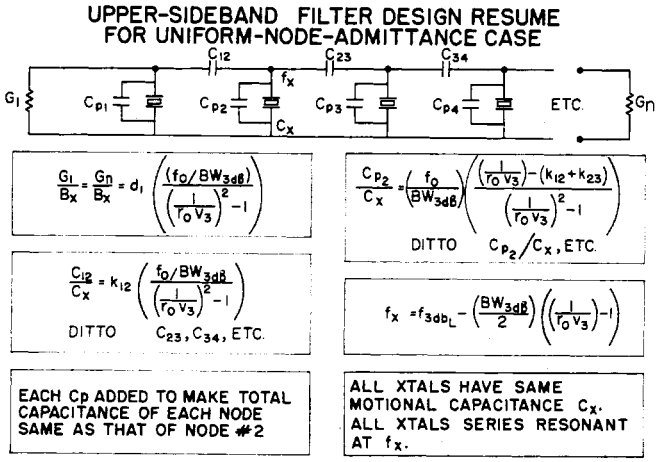

Fig. 9. The final upper sideband filter configuration and its element value design equations.

From Table I, we see that to produce this shape, $(k_{12}+k_{23})$ for the network must equal 1.77. Substitution of the preceding values into (31) shows that for this particular example the maximum attainable fractional bandwidth is 0.14 (C_x/C_h). As Table II, and the d and k tables and equations of [4] and [6] show, the required $(k_{12}+k_{23})$ decreases as the allowable peak-to-valley ratio in the pass band is increased; this fact, plus application of (31), shows that the maximum attainable fractional bandwidth can be appreciably increased by choosing a relative-attenuation shape having maximum allowable pass band ripple.

VI. Design Equations for a Lower Sideband Crystals-and-Capacitors-Only Filter

A. The Lower Sideband Relative-Attenuation Shape

For the lower sideband ladder filter shown in Fig. 10, (14a)–(14c), and all of the relative-attenuation data of Section IV, are directly applicable if the identifying names of "slow cutoff side," "return hill region," and "sharp cutoff edge" are used to identify the three frequency regions involved. Therefore, rather than redraw the graphs of that section, we will assume that the reader will properly identify the frequency regions involved when applying them to the lower sideband case.

B. Element Value Design Equations for the Case of Equal Mesh Impedance Levels

The element value equations given in Fig. 10 accomplish the practically desirable goal of requiring all crystals to have the same motional capacitance (C_x) having a reactance (X_x); and, in addition, are based on the specific procedure of making all the mesh impedance levels be the same and equal to X_0. These element value design equations are obtained by steps similar to those detailed in Section V.

The first element value equation,

$$X_0 = \frac{X_x}{[1 - |r_0 v_3|\,(k_{12}+k_{23})]^2} \tag{32}$$

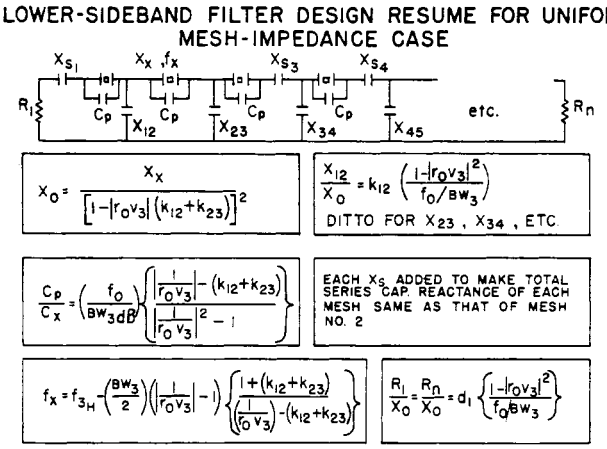

Fig. 10. The lower sideband filter configuration and its element value design equations.

fixes the mesh impedance level which must be used, once the actual crystal motional impedance is known, and the SSB relative-attenuation shape is picked. All crystals have this same motional reactance X_x.

The second element value equation, (33), fixes the capacitance (C_p) which must appear across the series-resonant circuit of each crystal.

$$\frac{C_p}{C_x} = \left(\frac{f_0}{BW_3}\right)\left\{\frac{\left|\frac{1}{r_0 v_3}\right| - (k_{12} + k_{23})}{\left|\frac{1}{r_0 v_3}\right|^2 - 1}\right\}. \tag{33}$$

This one capacitance value is across all the crystals, and, of course, to find the value of the actual physical capacitor which must be placed across each crystal unit, the crystal holder capacitance (C_h) must be subtracted from C_p.

Because (33) is identical to (29), the maximum physically realizable bandwidth discussion given in Section V-E applies also to this particular lower sideband filter design.

The third element value equation, (34), gives the required series-resonant frequency for all the crystals, in terms of arithmetic 3-dB-down mid-frequency f_m.

$$f_x = f_m + \left(\frac{BW_3}{2}\right)\left\{\frac{1 - \left|\frac{1}{r_0 v_3}\right|(k_{12} + k_{23})}{\left|\frac{1}{r_0 v_3}\right| - (k_{12} + k_{23})}\right\}. \tag{34}$$

All crystals have this same series-resonant frequency.

In the preceding three equations, the two adjacent normalized coefficients of coupling which are summed must be the two which (for the relative-attenuation shape chosen) give the largest sum. For the great majority of desirable shapes the largest sum will be that of $(k_{12}+k_{23})$ and, therefore, these are the two shown in the equations as given

The required value for each of the $(n-1)$ coupling capacitors is then calculated from

$$\frac{X_{12}}{X_0} = k_{12}\left[\frac{1 - |r_0 v_3|^2}{f_0/BW_3}\right] \tag{35}$$

with X_{23}, X_{34}, etc. and k_{23}, k_{34}, etc., replacing X_{12} and k_{12}, respectively.

Next, by adding the capacitors X_{s_r}, as in Fig. 10, the total capacitive reactance in each mesh (with the crystal unit figuratively removed) is made the same as that in the mesh having the largest total series capacitive reactance. For most desirable relative-attenuation shapes this largest total will occur in the second mesh, and this is the mesh referenced in the statement in Fig. 10. Equation (36) illustrates this step.

$$\begin{aligned} X_{s_1} &= (X_{12} + X_{23}) - X_{12} \\ X_{s_3} &= (X_{12} + X_{23}) - (X_{23} + X_{34}) \\ X_{s_4} &= (X_{12} + X_{23}) - (X_{34} + X_{45}) \\ &\text{etc.} \end{aligned} \tag{36}$$

Finally, the required loading resistors are calculated from

$$\frac{R_1}{X_0} = d_1\left[\frac{1 - |r_0 v_3|^2}{f_0/BW_3}\right] \tag{37}$$

with R_n and d_n replacing R_1 and d_1, respectively, to obtain the loading resistor required in the last mesh.

It is worth pointing out that the series capacitors X_s can always be properly associated with the adjacent shunt coupling capacitors to form T's of capacitance, which can then be transformed to equivalent π's. When this is done, every internal network node has a required capacitance both to ground and to the adjacent node, and there are then no unavoidable internal stray capacitances to ground, or otherwise, which cannot be properly absorbed in the network. Similarly, to end up with required capacitance to ground at the input and output terminals of the network, the parallel equivalent (over the small-percentage-bandwidth involved) of the series combination of R_1 and X_{s_1}, and R_n and X_{s_n} is used.

It should be stressed that the simple element value design equations of this section are for the case of equal mesh impedances and identical crystal units in each mesh; to simultaneously satisfy both these requirements, the series capacitors (C_s) of Fig. 10 are required. A design which still makes use of identical crystal units in each mesh, but does not require the series capacitors, can be accomplished by allowing each mesh to have a different impedance level.

VII. Conclusion

The derived frequency transformations of (9) and (14) enable the engineer to accurately and simply compute the SSB relative-attenuation shapes which can be obtained with the particular SSB ladder filters shown in Figs. 9 and 10. From the relative-attenuation graphs, Figs. 5–8, and the computation example of Table III,

plus the design procedure of Section IV-C, the engineer can straightforwardly find the number of crystal units, the pass band ripple, and the location of the infinite-attenuation frequency required to satisfy his SSB specification. Finally, from the element value design equations given in Sections V and VI and presented in Figs. 9 and 10, the engineer can accurately calculate the required value of all of the circuit elements involved.

References

[1] W. P. Mason, "Electric wave filters employing quartz crystals as elements," *Bell Sys. Tech. J.*, vol. 13, pp. 405–452, July 1934.
[2] R. A. Sykes, "A new approach to the design of high frequency crystal filters," 1958 *IRE Nat'l Conv. Rec.*, pt. 2, pp. 18–29.
[3] S. Darlington, "Synthesis of reactance 4-poles," *J. Math. Phys.*, vol. 18, pp. 257–353, September 1939.
[4] *Reference Data for Radio Engineers*, 4th ed. New York: International Telephone and Telegraph Corp., 1956, ch. 7, pp. 187–235.
[5] M. Dishal, "Gaussian response filter design," *Elect. Commun.*, vol. 36, no. 1, pp. 3–26, 1959.
[6] ——, "Two new equations for the design of filters," *Elect. Commun.*, vol. 30, pp. 324–337, December 1953; vol. 32, p. 178, September 1955.
[7] ——, "Design of dissipative band-pass filters producing desired exact amplitude-frequency characteristics," *Proc. IRE*, vol. 37, pp. 1050–1069, September 1949.
[8] W. E. Thomson, "Networks with maximally flat delay," *Wireless Engineer*, vol. 29, pp. 256–263, October 1952.

The Electromagnetic Propagation Characteristics of Venus and Mars

CHARLES E. FRANCIS, MEMBER IEEE

Abstract—**The information available about Mars and Venus and their atmospheres has been examined to determine the electromagnetic propagation characteristics of each planet. Consideration of some preliminary model atmospheres [6] indicates that the electromagnetic propagation effective radius of Venus is between 7400 and 13 900 km. Other models are discussed which give even larger effective radii and lead to the limit of a plane surface. The troposphere of Mars, because of its low density, was shown to have essentially no effect on the propagation loss between points on the surface or near the surface.**

An examination of the knowledge of the dielectric constants and conductivities of the surface revealed considerable uncertainties. Measured values of the dielectric constant are between 2.2 and 7.1 for the Venusian surface. The conductivity probably is 10^{-3} mhos/meter or less for both the Venusian and Martian surfaces if they have compositions similar to dry terrestrial soil. No measurement of the dielectric constant of the surface of Mars has been published.

Mars and Venus are strongly believed to have ionospheres in their atmospheres, but only crude estimations are available for the electron densities and the altitudes of these ionospheres.

I. Introduction

THE MODES of propagation of electromagnetic energy around Mars and Venus are basically the same as for Earth. The physical situation of all three is a sphere surrounded by an atmosphere. The spherical surfaces will have different values of curvature, dielectric constant, permeability, and conductivity. The atmospheres differ in amount, composition, and temperature, and the ionospheres are expected to exist in the upper regions.

Manuscript received September 28, 1964; revised April 1, 1965.
The author is with the Tucson Research Lab., Bell Aerosystems Co., Tucson, Ariz.

Much of the discussion in this paper will center around model atmospheres. Theories of atmospheres have been developed and are being improved. Certain bits of information about the atmospheres of planets have been obtained from spectroscopic, radiometric, and polarimetric measurements. The amount of solar radiation incident on a planet and its atmosphere can be determined from its distance from the sun. These bits of information have been combined with atmospheric theories [1] to determine model atmospheres. Considerable uncertainities exist in the data used, and the atmospheric theories are not as detailed as desired. No evaluations of any models are made in this paper; the ones selected for study are considered reasonable possibilities by most authorities.

The more general engineering problems of electromagnetic propagation at radio frequencies have been reduced to solution by using certain equations, tables, curves, and/or nomograms. The solutions to these problems require the knowledge of certain parameters, such as the electromagnetic effective planet radius, the dielectric constant and the conductivity of the surface material, and the effective dielectric constant, conductivity, and height of the ionosphere, which are known in varying degrees for Earth. The general purpose of this paper is to evaluate, where possible, these parameters for Venus and Mars and to show possible limiting values. Where the data are not available for any kind of evaluation, values that might be assumed are discussed. No propagation situations are computed.

Both the variation of the index of refraction in the tropospheres of Venus and Mars and the electromag-

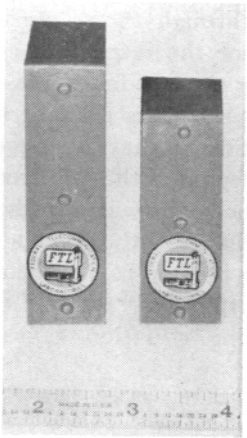

(a)

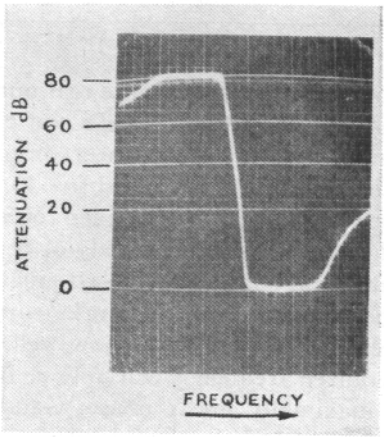

(b)

Fig. 1. (a) Lower (on left) and upper (on right) sideband crystals-and-capacitors-only SSB filters. (b) The swept relative attenuation on a logarithmic-attenuation scale of the upper sideband unit. The 80dB limitation is in the logarithmic measuring equipment, not in the filter.